Designing NSM FRP systems in concrete using partial safety factors

Mário Coelho[a], Luís Neves[b], José Sena-Cruz[a,*]

[a]*ISISE, University of Minho, Department of Civil Engineering, Campus de Azurém, 4810-058 Guimarães, Portugal*
[b]*University of Nottingham, Department of Civil Engineering, Nottingham, United Kingdom*

Abstract

This paper presents design procedures for fibre reinforced polymer (FRP) systems inserted in the cover of concrete elements according to the near-surface mounted (NSM) technique. Such strengthening system depends greatly on their bond strength. Two existing design formulations to estimate the bond strength of NSM FRP systems in concrete are studied. A reliability analysis is conducted with the purpose of making the design formulations consistent with the partial safety factors philosophy, including the Eurocodes. Hence, the necessary probabilistic distributions are calibrated based on a large database of bond tests. The results presented herein show that the existing guidelines can be extended and adopted under the framework of the Eurocodes. However, mainly due to their limitations in addressing individually all the possible failure modes, the variability of the probabilistic distributions found are quite high, leading to high partial coefficients of safety.

---

[*] Corresponding author

Email addresses: `mcoelho@civil.uminho.pt` (Mário Coelho), `luis.neves@nottingham.ac.uk` (Luís Neves), `jsena@civil.uminho.pt` (José Sena-Cruz)

Preprint submitted to Composites Part B *November 19, 2017*

Thus, in the future, new and improved formulations should be developed.

Keywords: FRP, NSM, Bond, Partial Safety Factors, Reliability

1. Introduction

This work is developed within the framework of strengthening concrete structures with fibre reinforced polymers (FRP). One of the most effective techniques to do so consists on the insertion of FRP bars into grooves opened on the concrete cover of the element to be strengthened. Typically, these FRP bars are fixed to concrete with an epoxy adhesive. These procedures are commonly designated as near-surface mounted technique (NSM). Despite the progress that has been made in the past years, design formulations to safely apply NSM FRP systems in the strengthening of concrete structures are still incipient [1, 2].

One of the most critical aspects regarding the NSM technique is related to the bond behaviour of the composite system [3], i.e. the stresses transfer between concrete and the FRP reinforcing bar. To better understand that behaviour, extensive bond tests have been carried out worldwide. Despite the existence of a manifold of test setups, those can be grouped in two main types: (i) direct and (ii) beam pullout tests [1]. In this work only the first type of pullout test setup is addressed as explained in further sections.

Considering the bond behaviour of a direct pullout specimen (see an example in Fig. 1), five local failure modes can be identified. Two have cohesive nature and occur either within the adhesive layer binding FRP to concrete (A) or into the concrete surrounding the groove (C). Other two failure modes have adhesive nature since they occur in the existing two interfaces, namely, between FRP and adhesive (F/A) or between adhesive and concrete (A/C). Finally, if none of the previous four failure modes occurred, failure will happen by FRP tensile rupture (F) [1].

In a previous work, a database of each one of the referred two types of bond tests was gathered [1]. Based on it, two of the most important guidelines for the design of NSM FRP systems were tested. One guideline is proposed for the design and construction of externally bonded FRP systems for strengthening concrete structures by the American Concrete Institute [4] referred in the present paper as ACI. The other is the Design handbook for reinforced concrete structures retrofitted with FRP and metal plates: beams and slabs from Standards Australia [5], referred herein as SA. Especially, the formulations included in these two guidelines to estimate the bond strength were analysed and improvements were suggested [1].

According to the authors' best knowledge, nowadays there are no European guidelines for NSM FRP systems, even though the draft version of the new annex of EN 1992-1-1 (Eurocode 2: Part 1-1) [6] refers to NSM FRP systems. On the other hand, the formulations to estimate the bond strength of NSM FRP systems included in both ACI and SA guidelines are not consistent with the partial safety factors framework.

Hence, this work presents a modification of ACI and SA formulations to, consistently with the partial safety factors methodology, yield designs with acceptable reliability indexes.

The philosophy behind the partial safety factors method recognizes that not all the designers should be familiar with reliability concepts which, in any case, must be followed in order to have safe structures. In the partial safety factor method, both actions and resistances are considered by their nominal values multiplied and divided, respectively, by partial safety factors. The way those partial factors are derived is responsible for introducing the reliability component into design. This means that, even without knowing, designers are indeed considering reliability in their projects. This philosophy is transversal to all EC thus, no matter what type of structure is being designed, the correspondent EC includes a set of partial factors to take into account the required reliability for all the design situations, designated as limit states, foreseen in that EC.

The Eurocode 0 (EC0) [7] describes in detail the background to the calibration of partial safety factors and the reliability analysis and targets used. Those are summarized in the next section.

2. Partial safety factors method

The objective of the partial safety factors method is to design structures resulting in a safety level, quantified by the reliability index, acceptable for society and similar for all types of structures. In the Eurocodes, for structures with a normal class of consequences, the target reliability index is defined equal to 3.8 for a fifty years reference period.

The reliability index is given by Eq. 1, where R is the resistance of the structure and E is the effect of actions. This probability can be computed using the first order reliability method (FORM). The reliability index is defined as the distance between the design point (i.e., the most likely failure point) and the origin in the normalized space, as shown in Fig. 2.

$$\beta = -\Phi^{-1}(p_f) = -\Phi^{-1}(P(R - E < 0)) \tag{1}$$

For a design corresponding to the lowest admissible value of the reliability index, the design point has coordinates $(-\alpha_R\beta; -\alpha_E\beta)$ in the normalized space. The corresponding resistance in the original space is such that $P(R = R_d) = \Phi(-\alpha_R\beta)$.

Although the values of the cosines α vary from design to design, a value of $\alpha_R = 0.8$ usually leads to acceptable results. Consequently, the design value of the resistance, R_d, can be computed according Eq. 2.

$$P\left(R = R_d\right) = \Phi\left(-\alpha_R\beta\right) = \Phi\left(-0.8 \times 3.8\right) \tag{2}$$

Once the probabilistic distribution of R is found, Eq. 2 can be used directly to compute the design point and, afterwards, to define partial safety factors that result in this design strength.

In the context of the present work, the partial safety factors method was adopted to calibrate ACI and SA formulations for predicting NSM FRP systems bond strength, using the database of direct pullout tests mentioned previously. To do that, the following main tasks were conducted:

(i) classify the specimens according their observed experimental failure mode and apply the corresponding theoretical limit state resistance function (R_t) to each specimen;

(ii) for each specimen, estimate the error (δ) of the theoretical resistance function using Eq. 3, where R_e is the experimental resistance value.

Then, adjust a probabilistic distribution to the theoretical resistance function errors obtained for all specimens;

$$\delta = R_e/R_t \tag{3}$$

(iii) compute the distribution of the probabilistic resistance function (R) defined in Eq. 4. If the only random variable in that function is the theoretical resistance function error, its probabilistic distribution can be estimated analytically. Otherwise, Monte Carlo simulation can be used to estimate the joint probabilistic distribution of all the random variables present in the probabilistic resistance function;

$$R = R_t\delta \tag{4}$$

(iv) compute the design value of the limit state resistance function (R_d). This should be obtained in order to have a probability of failure as defined in Eq. 5. In Eq. 5, α_R is the first order reliability method sensitivity factor for resistance and β is the reliability index. In this work those parameters were taken as 0.8 and 3.8, respectively, according to EC0 [7] suggestion;

$$P\left(R = R_t\delta \leq R_d\right) = \Phi\left(-\alpha_R\beta\right) \tag{5}$$

(v) rewrite the resistance function in its design form and define the safety factors to be included. This should be done taking into account that some variables are common to other applications foreseen in the EC and are expected to maintain the same partial safety factors throughout the EC;

(vi) replace (iv) in (v) and calibrate the values of the safety factors defined in the previous step.

The method explained above is similar to the generic approach of the design assisted by testing method, defined in the EC0 [7]. The main difference between them is that the method presented herein uses the probabilistic models of all the random variables, which can be of any type, and Monte Carlo simulations [8] to achieve the joint probabilistic distribution of the limit state resistance function in analysis. Contrarily, the design assisted by testing method defined in the EC0 is designed for resistance functions with normal and lognormal random variables which can be handled analytically.

The design assisted by testing method has already been successfully used in the context of RC members with FRP internal shear reinforcement [9] or with FRP applied by the externally bonded strengthening technique either to concrete [10–13] or to masonry [14]. However, according to authors' best knowledge, this paper presents the first attempt of applying it to calibrate the reliability parameters of the bond strength resistance functions suggested by ACI and SA, including the resistance models errors. In the following sections, the major details of the application and the obtained reliability parameters are presented.

3. Data and models

As previously referred, a database of direct and beam pullout tests was gathered in order to assess the accuracy of ACI and SA formulations to estimate the bond strength of NSM FRP systems in concrete [1]. Even though not always clear, the authors of the direct pullout tests presented a single critical experimental failure mode. Contrarily, in beam pullout tests, the authors normally provided several failure modes based on the final appearance of the tested specimen.

Since the failure mode needs to be clearly identified in the analyses carried herein, only direct pullout tests were selected for this study. Moreover, since the amount of tests using carbon FRP (CFRP) with rectangular cross-section is larger than the other types of FRP fibres/cross-sections, it was decided to conduct this work considering rectangular CFRP bars only.

Hence, Appendix A summarizes the main parameters of the 128 direct pullout tests that were used in the analyses presented in this work. They were grouped according to the failure mode obtained in the experimental tests. As it can be seen, all the possible five local failure modes (A, C, A/C, F/A and F) were found [1].

While in the analysis of ACI formulation all the 128 tests were used, with SA formulation some could not be used due to the lack of required information. Those specimens are identified in the notes of Appendix A.

3.1. Mechanical bond strength models

Table 1 summarizes the formulations to estimate NSM FRP systems bond strength suggested by ACI and SA guidelines (see notation section for details regarding the parameters included in this table). Both formulations are based on the assumption that a minimum development length (L_d) exists. If the existing bonded length (L_b) is equal or larger than L_d, the maximum pullout force (F_{fmax}) can be achieved. Otherwise, it should be reduced according to the actual bonded length.

ACI formulation estimates (F_{fmax}) considering two potential failure modes.

The first is associated with FRP rupture. The second failure mode is related with any debonding failure of the strengthening system, thus accounting for the failure modes A, C, F/A and A/C (see Fig. 1).

In turn, SA formulation considers three failure modes: (i) concrete cohesive failure; (ii) debonding failure of the strengthening system; (iii) FRP failure. Similarly to ACI formulation, the debonding failure includes failure within the adhesive or at one of the two interfaces.

In a previous work [1], both ACI and SA formulations were calibrated using a database of pullout tests more extensive than that used at the time both formulations were developed. Based on this, some modifications were suggested for both ACI and SA formulations in order to improve their prediction accuracy. Since it was proved that the pullout force depends on the FRP bar cross-section, the calibrations conducted in that work [1] considered the pullout tests separated according to the existing FRP bar cross-section. That database included pullout tests with rectangular, square and round FRP bars [1].

In this work, the modified ACI and SA formulations for pullout tests with FRP rectangular bars suggested in [1] were also analysed. The main purpose of this was to checking the effect of adopting more accurate formulations on the reliability analysis and partial safety factors discussed herein.

Regarding ACI, Coelho et al. [1] suggests that the value of the average bond strength (τ_{avg}) should be 9.25 MPa rather than 6.9 MPa, as recommended by ACI. Moreover, Coelho et al. [1] also proposed that τ_{avg} should not be constant but, alternatively, given by the ratio between FRP cross-section area (A_f) and the FRP/adhesive contact area, as shown in Eq. 6.

The latter area is defined by the product of the FRP perimeter (p_f) and the bonded length (L_b).

$$\tau_{avg} = 162 \left(\frac{A_f}{p_f L_b} \right)^{0.55} \tag{6}$$

Apart from these two differences in the assessment of τ_{avg}, no other changes were proposed to ACI formulation. This latter formulation, using Eq. 6, will be designated as "ACI modified" herein.

For the case of SA, the only improvement suggested in [1] resulted from recalibrating the expressions of its original formulation. The obtained expressions are not reproduced herein since, as will be further explained, the results obtained in the reliability analysis with those expressions are similar to the results obtained with the original expressions suggested in SA guideline and reproduced in Table 1.

3.2. Material probabilistic models

In order to conduct a reliability analysis it is necessary to define the probability distribution of all random variables. Three different probability distributions are considered in this paper, namely, normal (N), lognormal (LN) and Weibull (W); in what follows of this work they are presented as N,LN(mean; standard deviation) and $W(\alpha;\beta)$, respectively. In the Weibull distribution α is the scale parameter and β is the shape parameter.

It was considered that all the geometric parameters were deterministic, following the EC practice, while all mechanical parameters were considered as random variables. As shown in the previous section, ACI and SA formulations together require only three mechanical parameters, namely, FRP modulus of elasticity (E_f) and tensile strength (f_{fu}) and concrete compressive strength (f_c).

The probabilistic models for the first two parameters were obtained from the literature [15]. For both E_f and f_{fu} they consist of Weibull distributions as:

$$E_f \sim W\,(26.2; 180.9)\,\mathrm{GPa} \tag{7}$$

$$f_{fu} \sim W\,(15.9; 2777)\,\mathrm{MPa} \tag{8}$$

Regarding f_c, the adopted probabilistic model consisted on a lognormal distribution with 6% coefficient of variation, adapted from [16], as shown in Eq. 9. This distribution depends on the concrete class, thus the analyses were conducted taking into account the concrete mean compressive strength of each specimen according to the concrete classes defined in EC2 ($f_{cm,EC2}$) [6].

$$f_c \sim LN\,(f_{cm,EC2}; 0.06 f_{cm,EC2})\,\mathrm{MPa} \tag{9}$$

3.3. Probabilistic uncertainty for mechanical bond strength models

The uncertainty associated with the mechanical bond strength models, considered as a random variable, was defined by comparing the experimental maximum pullout force and the corresponding prediction according ACI and SA formulations.

Considering the mechanical bond models defined in section 3.1, it can be seen that, for both ACI and SA formulations, the theoretical limit state function associated with the FRP rupture (F) is defined by Eq. 10. This function was applied to the 32 specimens available in the database which presented FRP rupture failure mode.

$$R_{F(ACI/SA)} = A_f f_{fu} \tag{10}$$

Regarding ACI formulation, the remaining failure modes are all grouped in the debonding limit state (B). To obtain its theoretical function, the second branch of ACI formulation was firstly re-written by replacing L_d and τ_{avg} in F_{fmax} expression (see Table 1), as presented in Eq. 11. This expression was applied to the remaining 96 specimens.

$$R_{B(ACI)} = 6.9 L_b p_f \tag{11}$$

Regarding SA formulation, the theoretical limit state functions associated with concrete cohesive failure (C) and debonding failures (B) were also obtained by re-writing the expressions presented in Table 1 yielding to Eqs. 12 and 13, respectively. According to the failure modes reported in the database used, these functions were applied to 35 and 39 specimens, respectively.

$$R_{C(SA)} = \sqrt{0.73 \varphi_{per}^{0.5} f_c^{0.67} L_{per} E_f A_f} \tag{12}$$

$$R_{B(SA)} = \frac{2L_b}{\pi} \left(0.8 + 0.078 \varphi_{per}\right) L_{per} f_c^{0.6} \tag{13}$$

In addition to ACI and SA formulations, Eq. 14, corresponding to the ACI modified formulation referred in Eq. 6, was also used. It was applied to the same 96 specimens as Eq. 11.

$$R_{B(ACI\,modified)} = 162 \left(\frac{A_f}{p_f L_b}\right)^{0.55} L_b p_f \tag{14}$$

The expressions presented above, were applied to the corresponding specimens and the prediction errors were estimated as the ratio between experimental ($F_{fmax,Exp}$) and numerical ($F_{fmax,Num}$) pullout forces. Then, a probability distribution was fitted to the errors associated with each limit state.

Fig. 3 presents the probability distributions obtained for all limit state functions errors. The caption of each distribution includes also the corresponding probability parameters. It can be seen that, except for FRP rupture limit state, all other limit state errors were better fitted by lognormal distributions. This is mainly due to the asymmetry that those limit state functions present, and the need to guarantee a null probability of negative values for large coefficients of variation.

The coefficients of variation associated with the errors probability distributions were 8%, 53%, 18%, 61% and 30% for the limit states defined in Eqs. 10 to 14, respectively. Those are considerably high when compared with the coefficients of variation for the materials models which were 5%, 8% and 6%, for FRP modulus of elasticity and tensile strength and concrete compressive strength, respectively.

The results also show that ACI modified (Eq. 14) results in a significantly lower uncertainty than the original expression proposed by ACI (Eq. 11).

4. Safety factors calibration

Following the characterization of all random variables influencing the NSM FRP bond resistance, the partial safety factors were computed as described in section 2.

Table 2 summarizes the results obtained after applying the partial safety factors method to each limit state function. In the following paragraphs some specific aspects of each limit state analysis are highlighted, while in section 5 a critical analysis of the obtained results is presented.

Regarding the FRP rupture limit state, the expression to be used in design (R_d) is obtained from Eq. 10 by replacing CFRP tensile strength by its characteristic value (f_{fk}) divided by the partial safety factor of CFRP tensile stress (γ_f). This characteristic value was obtained by computing the 5% quantile of Eq. 8.

Regarding both ACI and modified ACI debonding limit states (which correspond to the same physical phenomenon), since only the average bond strength is not deterministic, in the sense that it is an assumed value, the reliability of the resistance function was applied to it.

Both concrete cohesive failure (C) and debonding (B) limit states of SA formulation depend on the concrete class. Hence, the results of these limit states were compiled in Table 3 per concrete class, considering all concrete classes available in the database used. Those concrete classes were estimated on the basis that the characteristic concrete strength could be obtained by subtracting 8 MPa to its mean value (provided by the authors of the experimental studies and shown in the Appendix A for each specimen) [6].

In both C and B limit states of SA formulation, the expression to be used in design is similar to their corresponding theoretical limit state functions. The only two differences are that concrete mean strength was replaced by its characteristic value (f_{ck}) divided by concrete's partial safety factor ($\gamma_c = 1.5$) [6] and that a new safety factor was added in each expression. This parameter behaves as a global safety factor and was computed per concrete class. The obtained values were also shown in Table 3.

4.1. Proposed design formulations

With the reliability parameters calibrated in the previous section, the expressions of ACI formulation presented in Table 1 should be replaced by Eqs. 15 and 16, in which $\gamma_f = 1.4$ and $\tau_d = 1.77$ MPa. Regarding the ACI modified formulation the only difference is that τ_d should be defined according to Eq. 17.

$$L_d = \frac{A_f \frac{f_{fk}}{\gamma_f}}{p_f \tau_d} \tag{15}$$

$$F_{fmax,d} = \begin{cases} A_f \frac{f_{fk}}{\gamma_f} \text{ if } L_b \geq L_d \\ A_f \frac{f_{fk}}{\gamma_f} \frac{L_b}{L_d} \text{ if } L_b < L_d \end{cases} \tag{16}$$

$$\tau_d = 61.6 \left(\frac{A_f}{p_f L_b} \right)^{0.55} \tag{17}$$

Similarly, SA formulation should be applied using Eqs. 18 to 20 to replace the corresponding ones in Table 1. In these equations $\gamma_f = 1.4$ and the parameters η_c and η_b should be taken from Table 3.

$$\tau_d = (0.8 + 0.078\varphi_{per}) \left(\frac{f_{ck}}{\gamma_c} \right)^{0.6} \tag{18}$$

$$\delta_d = \left[0.73\varphi_{per}^{0.5} \left(\frac{f_{ck}}{\gamma_c} \right)^{0.67} \right] / \tau_d \tag{19}$$

$$F_{fmax,d} = \begin{cases} \eta_c \sqrt{\tau_d \delta_d L_{per} E_f A_f} \leq A_f \frac{f_{fk}}{\gamma_f} \text{ if } L_b \geq L_d \\ \eta_b \sqrt{\tau_d \delta_d L_{per} E_f A_f} \frac{L_b}{L_d} \leq A_f \frac{f_{fk}}{\gamma_f} \text{ if } L_b < L_d \end{cases} \tag{20}$$

5. Results analysis

The results obtained in the reliability analysis presented in the previous sections are discussed in the following. The discussion begins by presenting in Section 5.1 the performance of the guidelines' original formulations in terms of failure mode prediction. Then, the remaining sections detail the major aspects related with the reliability analysis.

5.1. Specimens separated by guidelines' failure mode

According to EC philosophy, a theoretical resistance function should be developed based on the physics of the phenomenon in analysis. This means that the developed theoretical resistance function should be capable of predicting the real failure mode, even if the predicted strength results inaccurate.

To verify that aspect, both ACI and SA formulations as defined in the corresponding guidelines were applied to the database. Fig. 4 presents a comparison between the failure modes obtained in the experimental pullout tests (horizontal axis) and those predicted by ACI and SA guidelines (vertical axis). As can be seen, while in the experimental tests all the possible five failure modes occurred, in the guidelines' predictions only two failure modes were observed (F or B in ACI and C or B in SA). Remind that whilst this corresponds to all the failure modes that ACI considers, in the case of SA, the failure by FRP rupture was not predicted in any test.

Regarding ACI, it can be seen that its predictions fail more frequently when the real failure occurs by FRP rupture than when it occurs by one of the other four failure modes (all grouped in the debonding failure mode of ACI). Taking into account that the failure by FRP rupture is expected to occur for the highest pullout force that a specimen can sustain [1], when ACI predicts debonding and the real failure mode was FRP rupture, the prediction can be considered safe. Contrarily, when ACI predicts FRP rupture and the real failure occurred by any debonding mechanism, the prediction is unsafe. Hence, even though ACI fails more frequently when the real failure mode is FRP failure, the major problem is related with those specimens in which ACI predicted debonding failure and it actually occurred by FRP rupture.

Regarding SA, the first aspect to be mentioned is that, even though there are 32 specimens failing by FRP rupture in the database used, SA formulation did not predict any FRP rupture. Considering that the concrete failure is expected to occur for pullout forces larger than those occurring for any debonding failure (in SA this includes A, F/A and A/C) [1], the main problem regarding this formulation is also related with the prediction of debonding failure mode. In fact, there are several specimens in which the failure occurred by one of the three debonding mechanisms and SA predicted a failure within concrete.

5.2. Specimens separated by experimental failure mode

As already mentioned, a reliability analysis must be conducted taking into account the real failure mode occurred in each specimen. Hence, the specimens presented in Appendix A were separated by experimental failure mode regardless to the fact that, as referred in the previous section, the guidelines predict different failure modes in many cases.

Fig. 5 presents the relationship between experimental pullout force and that foreseen by each guideline for each specimen. Note that the later was obtained by applying directly the limit state function corresponding to the experimental failure mode and not the formulation as described in each guideline.

For both guidelines it can be seen that the limit state function related with FRP rupture (F) is the one presenting the lowest dispersion in the predictions. In the case of SA formulation, this dispersion was followed by the limit state functions for concrete cohesive failure (C) and, finally, debonding failure (B).

The limit state function associated with FRP rupture in NSM FRP systems coincides with the limit state function for the FRP rupture in tensile tests of FRP bars alone. The latter can be estimated using a classical and well established mechanical model (the product of the bar cross-section area by its normal strength). Hence, in this case, the dispersion of results should be mainly related with the different support conditions that exist in NSM FRP pullout tests when compared with those of a tension FRP bar test (together with the uncertainty in FRP mechanical properties).

The debonding limit state function addresses several failures using a single expression. Since the debonding mechanisms associated with each of these debonding failure modes are different, it is expectable that the same function predicts more accurately one of them and less accurately the reaming ones. This conclusion can be shown with the results in Fig. 5b. Since SA has an individual limit state function for concrete failure, its dispersion is lower than that found for debonding failures. Moreover, since ACI debonding limit state function addresses four failure modes while in SA it addresses three, the dispersion of predictions is larger in the former (Fig. 5a) than in the latter (Fig. 5b). This, naturally, has implications on the partial safety factors that were determined.

5.3. Bond strength according to the theoretical resistance models

Again according to the principals defined in EC0 [7], a theoretical resistance function should be capable of predicting the phenomenon it is representing on average. This means that, the value of the theoretical resistance function error (δ), expressed as the ratio between experimental ($F_{fmax,Exp}$) and numerical ($F_{fmax,Num}$) pullout forces, should have an average equal to one, being its distribution approximately symmetric. Fig. 6 presents the referred error obtained after applying both guideline's formulations to the database in Appendix A (red bars in each figure).

In both ACI (Fig. 6a) and SA (Fig. 6b) guidelines, about $\frac{1}{3}$ of predictions have a ratio inferior to one while the remaining $\frac{2}{3}$ stand above one. This means that both formulations are conservative, eventually already including some type of safety factors while those should be obtained *a posteriori*.

Contrarily, the modification proposed by the authors for ACI formulation (Fig. 6c) presents 45% and 55% of the predictions equal or below and above the unit, respectively, resulting in a centred prediction.

5.4. Partial safety factor for CFRP (γ_f)

From the available data the 32 specimens that failed by FRP rupture were used in the calibration of γ_f. Since both ACI and SA formulations present the same function for this limit state, a single value of $\gamma_f = 1.4$ was obtained for both guidelines.

According to EC philosophy, each material should have a single partial safety factor to be used in all the situations where that material can be applied and regardless to the resistance model being used. The obtained γ_f matches that requirement.

The value of γ_f found herein corresponds to an upper bound of those suggested in the literature. According to the authors' best knowledge, there are only two guidelines for the strengthening of concrete structures with FRP systems in which values of γ_f are explicitly provided.

The first one, referred herein as Italian guideline [17], addresses the strengthening using the externally bonded technique. It presents values of γ_f depending on the type of failure mode that can be influenced by the FRP properties. Hence, if the relevant failure mode is by FRP rupture (which is influenced by FRP properties) then its γ_f can be 1.1 or 1.25, depending on the type of certification of the strengthening system. If the critical failure mode is by debonding, γ_f can be 1.2 or 1.5, again depending on the certification type. Even though a single value should exist for γ_f, the authors of the Italian guideline decided for the use of different values for different limit states. Nevertheless, the important aspect is that the value suggested herein is in the range of those suggested by the Italian guideline thus harmonization of γ_f value could be easily achieved in the future.

The second guideline, is the Canadian Highway Bridge Design Code [18]. This guideline presents the values for γ_f in the form of a global factor to be applied to FRP tensile strength. It suggests the use of 0.85 for Aramid and Carbon FRP and 0.75 for glass FRP, corresponding to γ_f of 1.18 and 1.33, respectively, which are also similar to the value of 1.4 suggested herein.

5.5. ACI debonding safety factor (τ_d)

Regarding the debonding limit state defined by ACI guideline it was decided to guarantee the required safety margin by reducing the bond strength. This resulted in replacing the value of the average bond strength proposed in ACI, $\tau_{avg} = 6.9$ MPa, by its design value $\tau_d = 1.77$ MPa, calibrated in section 4. As referred before, this very large decrease (about 70%) in the bond strength results from the large uncertainty in the prediction models, a consequence of having a single expression addressing four different phenomena. Besides, as discussed in [1], the use of a single bond strength value, regardless of the FRP cross-section type, introduces a higher level of uncertainty than when the bond strength is estimated as a function of the FRP cross-section.

To verify that, the alternative designated ACI modified was also tested in this work (see section 4). The design bond strength obtained with that different and more accurate model was about 60% lower than the original value. This smaller reduction proves that, even if a single limit state function is used to address all four failure modes, a more accurate prediction model can result in a significant increase in design strength.

5.6. SA global safety factors (η_c and η_b)

Regarding SA limit states related with concrete and debonding failure modes, it was decided to provide them with reliability features by applying global safety factors. The reason for this decision is related with the type of variables their resistance functions include. Besides geometry variables, which are treated as deterministic, both resistance functions contain two mechanical variables only. Namely, the compressive strength of concrete and the FRP modulus of elasticity (just in concrete limit state).

Regarding concrete compressive strength, it already has a well-established partial safety factor of 1.5 which, according to EC philosophy, should be maintained in all the applications of concrete material. Regarding the FRP modulus of elasticity, it is not usual to affect the elasticity modulus of a material with partial factors. Instead, the usual procedure consists on applying such factors to material's stresses and strains thus, by Hooke's law, the elasticity modulus remains unaffected by safety factors. In order to maintain this approach, thus addressing the compatibility between codes recommended by EC, it was also decided to do not apply partial safety factor to the FRP modulus of elasticity.

Hence, the solution adopted was the use of global safety factors as defined in section 4 for concrete and debonding limit states. As expected, comparing the magnitude of values obtained, it can be seen that the safety factors are lower for debonding than for concrete limit state. This is mainly related with the former addressing several failure modes, as mentioned before.

For design purposes it would be better to have a single global safety factor for each limit state, regardless to the concrete class. In fact, EC also presents a single partial safety factor for concrete regardless to its class. On the other hand, the global safety factors obtained herein (see Table 3) are quite similar, thus the lowest value of each safety factor can be used for each limit state and for all concrete classes. The impact of this option would be a more conservative design for those specimens using concrete classes bellow C55/67, which is the class presenting the lowest global safety factors.

5.7. Bond strength in the theoretical resistance models with reliability parameters

Contrarily to what was referred before for the theoretical models, the models with reliability parameters are not expected to necessarily predict the real failure mode. In fact, these models will produce prediction values lower than the real ones, thus safer.

Fig. 6 presents, as blue bars, the ratio between the experimental maximum pullout force and that estimated using the proposed design formulations (including the corresponding safety factors). The obtained results show, as expected, that all these ratios are larger than one. The only exception occurs for SA guideline (see Fig. 6b) where only one specimen attained a ratio of 0.94 mainly due to decimals rounding.

Comparing the magnitude of the ratios obtained, those are in agreement with the reliability parameters estimated for each formulation. The higher the reductions applied to each limit state function, the larger the ratios are. It should be mentioned that, from a design viewpoint, larger ratios correspond to less economical designs, thus it would be better if the ratios were as small as possible, yet larger than one.

Concerning ACI formulation as defined in the guideline (Fig. 6a) or its modified version (Fig. 6c), it can be confirmed that the lower reduction on the design bond strength associated with the better accuracy of the latter, resulted in less conservative predictions. In other words, the blue bars in Fig. 6a present a larger dispersion and are available in larger numbers in the right side of the figure than the ones shown in Fig. 6c.

Regarding SA guideline (Fig. 6b), the ratios are lower than 2.5 for about

40% of the specimens while for the remaining specimens the ratios increase up to 16.5. This should be related with the global reliability parameters applied for concrete and debonding failure limit states in SA formulation. In fact, the reductions applied to these limit states were as high as 35% and 77% of their theoretical prediction, respectively. This emphasizes the fact that safety factors should be applied to individual material properties, rather than to the entire resistance function.

5.8. Probability models adopted for CFRP parameters

Despite the considerable range of the two CFRP properties required in the resistance models analysed in this work ($E_f = [123 - 182]$ GPa, $f_{fu} = [1850 - 3100]$ MPa), the same model was used for each parameter and for all specimens. Even though this could seem to be a limitation of the present study, the range of values referred above are within the range of values used in the development of the probabilistic models for CFRP properties used herein. Eqs. 7 and 8 were defined by using CFRP bars with E_f ranging between 118 to 218 GPa and f_{fu} ranging between 1780 to 3310 MPa [15]. Note that these CFRP bars correspond to a single brand from a single manufacturer. However, assuming that the production processes adopted by different manufacturers would be similar, the coefficients of variation regarding E_f and f_{fu} for other CFRP bars' brands, should be also similar, differing mainly in the average values.

It has been proved that CFRP tensile properties (E_f and f_{fu}) are well described by Weibull probability distributions [15, 19–21], which have a coefficient of variation, c_v, estimated according Eq. 21, where Γ is the Gamma function and α is the Weibull distribution scale parameter. In the Weibull distributions presented in Eqs. 7 and 8 it can be seen that the shape parameter β (which does not appear in the expression of c_v) roughly coincides with the average value of each property.

$$c_v = \frac{\sqrt{\Gamma\left(1+\frac{2}{\alpha}\right) - \Gamma^2\left(1+\frac{1}{\alpha}\right)}}{\Gamma\left(1+\frac{1}{\alpha}\right)} \tag{21}$$

Taking all of these into account, it can be assumed that since different CFRP brands would have different mechanical properties average values (related with the material composition) but similar coefficients of variation (related with the fabrication process), and that the average value has no influence on the coefficient of variation, the same model can be used for different CFRP brands, which validates the analyses presented in this work.

In any case, the results obtained in this work were found satisfactory. In the future, as new probabilistic models for these CFRP parameters become available, the analyses presented herein can be easily updated and these assumptions validated.

5.9. Influence of the mechanical model

As referred in section 3.1, in a previous work both ACI and SA were recalibrated [1]. Namely, in the case of ACI formulation its average bond strength value was recalibrated. In the case of SA formulation the expressions that were developed by SA authors based on experimental data were also recalibrated. This includes the expressions for τ_{max} and δ_{max} (see Table 1).

These recalibrated formulations were also object of a reliability analysis using the methodology described in this work.

Regarding ACI, the recalibrated average bond strength value was equal to 9.25 MPa. As expected, it was found that the use of this value in the theoretical resistance function lead to the same value of $\tau_d = 1.77$ MPa in the design function. In fact, using 9.25, 6.9 or any other scalar as theoretical average bond strength, would lead to the same average bond strength design value. Using different scalars, one is just shifting the mean of the error being the coefficient of variation the same. Hence, unless the latter, which is the important statistical parameter in the reliability analyses, significantly changes, the design value would always be the same regardless to the theoretical value adopted.

An example of that change could be achieved by replacing the scalar average bond strength by an expression. That was already verified before when the ACI modified version was presented. In the end, the resistance design values obtained for ACI formulation with any scalar (6.9, 9.25, ... MPa) was always 0.26 while it increased to 0.39 for ACI modified version.

Regarding SA, the recalibrated expressions lead also to similar design values. In fact, the mechanical models were the same, but with lower average prediction errors. Hence, only the original version of this formulation was referred in the previous sections.

6. Conclusions

This paper presented a reliability analysis over two of the most important guidelines for the design of concrete structures strengthened with NSM FRP systems. A formulation for calibrating the reliability parameters necessary to make the referred guidelines consistent with the partial safety factors philosophy was shown and the correspondent reliability parameters deduced.

From the work presented herein, the following major conclusions can be drawn:

- the absence of probabilistic models for the different types of FRP limited this study to carbon FRP. A large scale analysis of the probabilistic models for FRP properties is paramount for defining reliable design codes;

- the amount of experimental data available is still very low. This has direct influence in the definition of the errors associated with each limit state function. For this reason, in this work only direct pullout specimens with CFRP rectangular bars were considered. Hence, it is necessary to continue performing direct pullout tests, specially using combinations of parameters and materials that were not tested yet;

- due to the non-existence of a standard NSM FRP direct pullout test, part of the theoretical resistance models errors should be associated with the differences between tests conditions rather than with the models. In fact, aspects like specimen size, setup configuration or even support conditions could influence the experimental maximum pullout force value. That will naturally also influence the magnitude of the errors associated with the perdition models. Hence, the definition of a standard NSM FRP direct pullout test is urgent;

- while in the case of ACI formulation it was possible to define reliability parameters affecting directly specific properties (either FRP tensile strength or strengthening system bond strength), in the case of SA the reliability had to be included by means of global safety factors in order to maintain the partial safety factor of concrete in agreement with that already in the Eurocodes;

- it was confirmed that, mainly due to the difficulty of ACI and SA guidelines to predict separately all the five local failure modes existing in a NSM FRP system, more accurate resistance models should be developed for estimating the bond strength of NSM FRP systems in the future;

- finally, regardless to the limitations of ACI and SA guidelines, the necessary reliability parameters were estimated and can be used in order to design NSM FRP systems according to Eurocodes philosophy, thus attaining a strengthening with the reliability index recommended by Eurocodes.

Acknowledgements

This work was supported by FEDER funds through the Operational Program for Competitiveness Factors – COMPETE and National Funds through FCT (Portuguese Foundation for Science and Technology) under the project CutInDur FCOMP-01-0124-FEDER-014811 (ref. PTDC/ECM/112396/2009) and partly financed by the project POCI-01-0145-FEDER-007633. The first author wishes also to acknowledge the Grant No. SFRH/BD/87443/2012 provided by FCT.

Appendix A.

The following table contains the data used in the analyses presented in this paper.

Paper ID	Specimen ID	b_g [mm]	d_g [mm]	L_b [mm]	f_{cm} [MPa]	p_f [mm]	A_f [mm^2]	E_f [GPa]	f_{fu} [MPa]	F_{fmax} [kN]
FRP tensile rupture failure mode, F (32 specimens)										
[22]	48 MPa-200-10	3.28	12.10	200.00	48.20	22.76	12.93	161.80	2643.00	33.70
[22]	49 MPa-200-10	3.26	12.56	200.00	49.20	23.64	13.31	161.80	2643.00	33.30
[22]	49 MPa-200-20	3.28	22.43	200.00	49.20	43.42	26.15	162.30	2796.00	68.60
[22]	49 MPa-300-20	3.24	21.79	300.00	49.20	42.06	24.54	162.30	2796.00	68.10
[22]	53 MPa-200-20	3.26	22.47	200.00	52.80	43.46	25.79	162.30	2796.00	77.90
[22]	53 MPa-200-20	3.27	22.10	200.00	53.00	42.74	25.53	162.30	2796.00	72.50
[22]	53 MPa-100-10	3.26	12.37	100.00	53.00	23.26	13.07	161.80	2643.00	29.50
[22]	53 MPa-300-10	3.27	12.30	300.00	53.00	23.14	13.08	161.80	2643.00	37.90
[22]	53 MPa-300-20	3.25	22.15	300.00	53.00	42.80	25.19	162.30	2796.00	66.30
[22]	33 MPa-300-20	3.24	21.85	300.00	33.40	42.18	24.61	162.30	2796.00	67.80
[23]	C-1.4x10-S-1	5.00	15.00	300.00	18.40	22.80	14.00	177.00	2221.00	31.16
[23]	C-1.4x10-S-2	5.00	15.00	300.00	18.40	22.80	14.00	177.00	2221.00	32.93
[23]	C-1.4x10-S-3	5.00	15.00	300.00	18.40	22.80	14.00	177.00	2221.00	34.73

Continued on next page

Continued from previous page

Paper ID	Specimen ID	b_g [mm]	d_g [mm]	L_b [mm]	f_{cm} [MPa]	p_f [mm]	A_f [mm^2]	E_f [GPa]	f_{fu} [MPa]	F_{fmax} [kN]
[24]	8-31[R/60/L/6.4p]	10.00	24.00	230.00	56.24	36.00	32.00	123.00	2043.00	61.60
[24]	8-31[R/60/L/6.4p]c	10.00	24.00	230.00	56.24	36.00	32.00	123.00	2043.00	62.10
[25]	Lb90X12_a	5.00	22.00	90.00	25.03	22.02	13.86	156.10	2879.00	37.32
[25]	Lb90X12_b	5.00	22.00	90.00	25.03	22.02	13.86	156.10	2879.00	34.61
[25]	Lb120X12_a	5.00	22.00	120.00	25.03	22.02	13.86	156.10	2879.00	37.95
[25]	Lb150X12_b	5.00	22.00	150.00	25.03	22.02	13.86	156.10	2879.00	38.39
[25]	Lb90X6_a	5.00	22.00	90.00	25.03	22.02	13.86	156.10	2879.00	34.38
[25]	Lb90X6_b	5.00	22.00	90.00	25.03	22.02	13.86	156.10	2879.00	33.50
[25]	Lb120X6_a	5.00	22.00	120.00	25.03	22.02	13.86	156.10	2879.00	36.15
[25]	Lb120X6_a	5.00	22.00	120.00	25.03	22.02	13.86	156.10	2879.00	34.26
[25]	Lb150X6_b	5.00	22.00	150.00	25.03	22.02	13.86	156.10	2879.00	36.47
[25]	Lb120X0_a	5.00	22.00	120.00	25.03	22.02	13.86	156.10	2879.00	33.78
[25]	Lb120X0_b	5.00	22.00	120.00	25.03	22.02	13.86	156.10	2879.00	35.39
[25]	Lb150X0_a	5.00	22.00	150.00	25.03	22.02	13.86	156.10	2879.00	37.29
[25]	Lb150X0_b	5.00	22.00	150.00	25.03	22.02	13.86	156.10	2879.00	32.05

Continued on next page

Continued from previous page

Paper ID	Specimen ID	b_g [mm]	d_g [mm]	L_b [mm]	f_{cm} [MPa]	p_f [mm]	A_f [mm^2]	E_f [GPa]	f_{fu} [MPa]	F_{fmax} [kN]
[26]*	TS1-3.6-C20	NA	25.00	350.00	38.80	27.20	36.00	165.00	2700.00	79.60
[26]*	TS1-3.6-C20R	NA	25.00	350.00	38.80	27.20	36.00	157.00	2700.00	95.00
[26]*	TS1-3.6-C30	NA	35.00	350.00	38.80	27.20	36.00	156.00	2700.00	101.80
[26]*	TS1-3.6-C40	NA	45.00	350.00	38.80	27.20	36.00	160.00	2700.00	105.70
Cohesive failure mode at concrete, C (50 specimens)										
[22]	30 MPa-100-10b	3.20	12.00	100.00	30.00	22.40	12.00	161.80	2643.00	22.60
[22]	30 MPa-100-10	3.22	12.02	100.00	30.00	22.48	12.22	161.80	2643.00	20.40
[22]	30 MPa-150-10	3.23	12.33	150.00	30.00	23.12	12.71	161.80	2643.00	23.20
[22]	30 MPa-200-10	3.22	12.48	200.00	30.00	23.40	12.79	161.80	2643.00	27.90
[22]	30 MPa-250-10	3.22	12.29	250.00	30.00	23.02	12.55	161.80	2643.00	26.60
[22]	30 MPa-300-10	3.22	12.38	300.00	30.00	23.20	12.66	161.80	2643.00	26.00
[22]	30 MPa-350-10	3.22	12.35	350.00	30.00	23.14	12.63	161.80	2643.00	23.00
[22]	42 MPa-200-10	3.27	12.29	200.00	41.80	23.12	13.07	161.80	2643.00	30.60
[22]	30 MPa-100-20	3.20	22.00	100.00	30.00	42.40	24.00	162.30	2796.00	51.40
[22]	30 MPa-200-20	3.20	22.00	200.00	30.00	42.40	24.00	162.30	2796.00	57.80

Continued on next page

Continued from previous page

Paper ID	Specimen ID	b_g [mm]	d_g [mm]	L_b [mm]	f_{cm} [MPa]	p_f [mm]	A_f [mm^2]	E_f [GPa]	f_{fu} [MPa]	F_{fmax} [kN]
[22]	30 MPa-300-20	3.20	22.00	300.00	30.00	42.40	24.00	162.30	2796.00	66.70
[22]	65 MPa-200-10	4.88	12.08	200.00	64.80	25.92	29.03	144.60	2634.00	45.00
[22]	65 MPa-200-20	4.97	21.77	200.00	64.80	45.48	58.72	162.30	2796.00	108.80
[22]	53 MPa-200-10	3.24	12.23	200.00	52.80	22.94	12.69	161.80	2643.00	31.90
[22]	53 MPa-200-10	3.30	12.43	200.00	53.00	23.46	13.56	161.80	2643.00	34.00
[22]	53 MPa-100-20	3.25	22.23	100.00	53.00	42.96	25.29	162.30	2796.00	63.80
[22]	33 MPa-200-15	3.26	17.65	200.00	33.40	33.82	19.72	162.05	2643.00	47.10
[22]	33 MPa-300-15	3.26	17.31	300.00	33.40	33.14	19.29	162.05	2643.00	51.60
[22]	65 MPa-200-10	4.90	11.95	200.00	64.80	25.70	28.86	144.60	2634.00	45.10
[22]	33 MPa-200-20	3.20	22.00	200.00	33.40	42.40	24.00	162.30	2796.00	52.40
[27]	P2	5.00	20.00	300.00	50.00	36.00	45.00	157.00	2580.00	57.30
[27]	P4	5.00	20.00	300.00	50.00	36.00	45.00	157.00	2580.00	56.74
[27]	P6	5.00	25.00	300.00	50.00	45.00	50.00	153.00	2500.00	62.40
[28]	E-RT-1	6.40	21.00	152.00	40.70	36.00	32.00	141.50	2775.50	50.60
[28]	E-RT-2	6.40	21.00	152.00	40.70	36.00	32.00	141.50	2775.50	52.20

Continued on next page

Continued from previous page

Paper ID	Specimen ID	b_g [mm]	d_g [mm]	L_b [mm]	f_{cm} [MPa]	p_f [mm]	A_f [mm^2]	E_f [GPa]	f_{fu} [MPa]	F_{fmax} [kN]
[28]	E-RT-3	6.40	21.00	152.00	40.70	36.00	32.00	141.50	2775.50	55.40
[28]	E-RT-4	6.40	21.00	152.00	40.70	36.00	32.00	141.50	2775.50	55.70
[29]	G0NSM1	3.00	21.00	350.00	35.50	42.40	24.00	161.00	2720.00	61.20
[29]	G0NSM2	3.00	21.00	350.00	35.50	42.40	24.00	161.00	2720.00	64.80
[30]	N150-1	7.10	20.00	150.00	24.00	39.20	57.60	160.00	2800.00	88.26
[30]	N200-1	7.10	20.00	200.00	24.00	39.20	57.60	160.00	2800.00	90.21
[25]	Lb70X0_a	5.00	22.00	70.00	25.03	42.80	28.00	165.00	1850.00	36.53
[25]	Lb70X0_b	5.00	22.00	70.00	25.03	42.80	28.00	165.00	1850.00	34.58
[25]	Lb90X0_a	5.00	22.00	90.00	25.03	42.80	28.00	165.00	1850.00	42.00
[25]	Lb90X0_b	5.00	22.00	90.00	25.03	42.80	28.00	165.00	1850.00	41.70
[29]**	C150NSMb	NA	NA	350.00	35.50	84.80	96.00	173.00	2720.00	205.10
[26]**	TS1-3.6-C0	NA	5.00	350.00	38.80	27.20	36.00	150.00	2700.00	40.00
[26]**	TS1-3.6-C0R	NA	5.00	350.00	38.80	27.20	36.00	160.00	2700.00	39.20
[26]**	TS1-3.6-C10	NA	15.00	350.00	38.80	27.20	36.00	165.00	2700.00	61.80
[26]**	TS2-6.0-C0	NA	5.00	350.00	38.80	32.00	60.00	166.00	2700.00	54.80

Continued on next page

Continued from previous page

Paper ID	Specimen ID	b_g [mm]	d_g [mm]	L_b [mm]	f_{cm} [MPa]	p_f [mm]	A_f [mm^2]	E_f [GPa]	f_{fu} [MPa]	F_{fmax} [kN]
[26]**	TS2-6.0-C10	NA	15.00	350.00	38.80	32.00	60.00	165.00	2700.00	86.10
[26]**	TS2-6.0-C20	NA	25.00	350.00	38.80	32.00	60.00	169.00	2700.00	136.00
[26]**	TS2-6.0-C30B	NA	35.00	350.00	38.80	32.00	60.00	159.00	2700.00	108.80
[26]**	TS2-6.0-C50	NA	55.00	350.00	38.80	32.00	60.00	NA	2700.00	81.80
[26]**	TS2-6.0-C55	NA	60.00	350.00	38.80	32.00	60.00	160.00	2700.00	138.20
[26]**	TS3-6.0-C15	NA	20.00	350.00	38.80	32.00	60.00	160.00	2700.00	89.80
[26]**	TS3-6.0-C25	NA	30.00	350.00	38.80	32.00	60.00	161.00	2700.00	117.00
[26]**	TS3-6.0-C30	NA	35.00	350.00	38.80	32.00	60.00	160.00	2700.00	129.90
[26]**	TS3-6.0-C40	NA	45.00	350.00	38.80	32.00	60.00	154.00	2700.00	130.60
[26]**	TS3-6.0-C50	NA	45.00	350.00	38.80	32.00	60.00	NA	2700.00	90.00
Cohesive failure mode at adhesive, A (10 specimens)										
[22]	49 MPa-100-20	3.27	22.37	100.00	49.20	43.28	25.87	162.30	2796.00	64.10
[22]	49 MPa-200-20	3.28	22.22	200.00	49.20	43.00	25.88	162.30	2796.00	75.00
[22]	33 MPa-100-15	3.26	16.93	100.00	33.40	32.38	18.81	162.05	2643.00	31.90
[31, 32]	C_STR_2x16	8.00	25.00	300.00	35.00	36.00	32.00	124.00	2068.00	46.50

Continued on next page

Continued from previous page

Paper ID	Specimen ID	b_g [mm]	d_g [mm]	L_b [mm]	f_{cm} [MPa]	p_f [mm]	A_f [mm^2]	E_f [GPa]	f_{fu} [MPa]	F_{fmax} [kN]
[24]	7-25[R/60/S/1.6p]	6.00	20.00	58.00	57.52	36.00	32.00	123.00	2043.00	28.10
[24]	7-26[R/60/S/3.2p]	6.00	20.00	115.00	55.68	36.00	32.00	123.00	2043.00	34.30
[24]	7-27[R/60/S/6.4p]	6.00	20.00	230.00	55.68	36.00	32.00	123.00	2043.00	50.80
[24]	7-28[R/60/S/12.7p]	6.00	20.00	460.00	49.92	36.00	32.00	123.00	2043.00	57.10
[24]	8-29[R/60/L/1.6p]	10.00	24.00	58.00	56.24	36.00	32.00	123.00	2043.00	26.20
[24]	8-30[R/60/L/3.2p]	10.00	24.00	115.00	57.52	36.00	32.00	123.00	2043.00	43.40
FRP/Adhesive interface failure mode, F/A (19 specimens)										
[33]	CS-200	9.00	22.00	200.00	23.20	40.00	64.00	151.00	2068.00	54.50
[33]	CS-250	9.00	22.00	250.00	23.20	40.00	64.00	151.00	2068.00	64.00
[31, 32]	C-2.5x15-S1	8.00	25.00	300.00	34.00	35.00	37.50	165.00	3100.00	60.60
[31, 32]	C-2.5x15-S2	8.00	25.00	300.00	34.00	35.00	37.50	165.00	3100.00	60.90
[31, 32]	C-2.5x15-S3	8.00	25.00	300.00	34.00	35.00	37.50	165.00	3100.00	58.10
[25]	Lb40X12_a	5.00	22.00	40.00	25.03	22.02	13.86	156.10	2879.00	19.93
[25]	Lb40X12_b	5.00	22.00	40.00	25.03	22.02	13.86	156.10	2879.00	19.81
[25]	Lb70X12_a	5.00	22.00	70.00	25.03	22.02	13.86	156.10	2879.00	31.43

Continued on next page

Continued from previous page

Paper ID	Specimen ID	b_g [mm]	d_g [mm]	L_b [mm]	f_{cm} [MPa]	p_f [mm]	A_f [mm^2]	E_f [GPa]	f_{fu} [MPa]	F_{fmax} [kN]
[25]	Lb70X12_b	5.00	22.00	70.00	25.03	22.02	13.86	156.10	2879.00	29.40
[25]	Lb40X6_a	5.00	22.00	40.00	25.03	22.02	13.86	156.10	2879.00	18.58
[25]	Lb40X6_b	5.00	22.00	40.00	25.03	22.02	13.86	156.10	2879.00	18.59
[25]	Lb70X6_a	5.00	22.00	70.00	25.03	22.02	13.86	156.10	2879.00	27.70
[25]	Lb70X6_b	5.00	22.00	70.00	25.03	22.02	13.86	156.10	2879.00	26.74
[25]	Lb90X0_a	5.00	22.00	90.00	25.03	22.02	13.86	156.10	2879.00	27.92
[25]	Lb90X0_b	5.00	22.00	90.00	25.03	22.02	13.86	156.10	2879.00	27.80
[25]	Lb50X0_a	5.00	22.00	50.00	25.03	42.80	28.00	165.00	1850.00	31.27
[25]	Lb50X0_b	5.00	22.00	50.00	25.03	42.80	28.00	165.00	1850.00	31.55
[34]	Rectangular_200	6.00	25.00	200.00	34.86	42.80	28.00	165.00	2300.00	24.00
[34]	Rectangular_250	6.00	25.00	250.00	34.86	42.80	28.00	165.00	2300.00	31.00
Adhesive/Concrete interface failure mode, A/C (17 specimens)										
[23]	C-2.5x15-S-1	8	25	300	18.4	35	37.5	182	2863	52.97
[23]	C-2.5x15-S-2	8	25	300	18.4	35	37.5	182	2863	56.03
[23]	C-2.5x15-S-3	8	25	300	18.4	35	37.5	182	2863	46.26

Continued on next page

Continued from previous page

Paper ID	Specimen ID	b_g [mm]	d_g [mm]	L_b [mm]	f_{cm} [MPa]	p_f [mm]	A_f [mm^2]	E_f [GPa]	f_{fu} [MPa]	F_{fmax} [kN]
[35]	C1.4x10S-1	4.64	15.54	300	34.8	22.8	14	165	1850	36.6
[35]	C1.4x10S-2	4.64	15.54	300	34.8	22.8	14	165	1850	39.4
[35]	C1.4x10S-3	4.64	15.54	300	34.8	22.8	14	165	1850	41.4
[35]	C2.5x15S	7.65	23.56	300	34.8	35	37.5	165	3100	49.6
[35]	C2.5x15S	7.65	23.56	300	34.8	35	37.5	165	3100	48.3
[35]	C2.5x15S	7.65	23.56	300	34.8	35	37.5	165	3100	48
[34]	Rectangular_300	6	25	300	34.86	42.8	28	165	2300	51
[26]**	TS2-6.0-C40	NA	45	350	38.8	32	60	153	2700	150
[36]**	DP600NS-1	6.4	19	152	NA	36	32	130	2500	43.6
[36]**	DP600NS-2	6.4	19	152	NA	36	32	130	2500	54.3
[36]**	DP600NS-3	6.4	19	152	NA	36	32	130	2500	50.7
[36]**	DP600NS-4	6.4	19	152	NA	36	32	130	2500	41.8
[36]**	DP600NS-5	6.4	19	152	NA	36	32	130	2500	48
[36]**	DP600NS-6	6.4	19	152	NA	36	32	130	2500	48

Notes: * specimens not used in the analyses with SA formulation as in this guideline but used in the analyses with SA by failure mode; ** specimens not used in the analyses with SA formulation as in the guideline nor in the analyses with SA by failure mode.

References

[1] Coelho M, Sena-Cruz J, Neves L. A review on the bond behavior of FRP NSM systems in concrete. Construction and Building Materials 2015;93:1157–69. URL http://dx.doi.org/10.1016/j.conbuildmat.2015.05.010.

[2] Zhang S, Yu T, Chen G. Reinforced concrete beams strengthened in flexure with near-surface mounted (NSM) CFRP strips: Current status and research needs. Composites Part B: Engineering 2017;131:30–42. URL http://dx.doi.org/10.1016/j.compositesb.2017.07.072.

[3] Breveglieri M, Aprile A, Barros J. RC beams strengthened in shear using the Embedded Through-Section technique: Experimental results and analytical formulation. Composites Part B: Engineering 2016;89:266–81. URL http://dx.doi.org/10.1016/j.compositesb.2015.11.023.

[4] ACI. Guide for the design and construction of externally bonded FRP systems for strengthening concrete structures. 4402R-08; American Concrete Institute, Farmington Hills, MI, USA; 2008.

[5] SA. Design handbook for RC structures retrofitted with FRP and metal plates: beams and slabs. HB 305-2008; Standards Australia GPO Box 476, Sydney, NSW 2001, Australia; 2008.

[6] CEN. Eurocode 2: Design of concrete structures. EN 1992-1-1:2004 E; Comité Européen de Normalisation, Bruxeles; 2004.

[7] CEN. Eurocode 0: Basis of structural design. EN 1990:2002 E; Comité Européen de Normalisation, Bruxeles; 2002.

[8] Bianco V, Monti G, Barros J. Design formula to evaluate the NSM FRP strips shear strength contribution to a RC beam. Composites Part B: Engineering 2014;56:960–71. URL http://dx.doi.org/10.1016/j.compositesb.2013.09.001.

[9] Lignola G, Jalayer F, Nardone F, Prota A, Manfredi G. Probabilistic design equations for the shear capacity of RC members with FRP internal shear reinforcement. Composites Part B: Engineering 2014;67:199–208. URL http://dx.doi.org/10.1016/j.compositesb.2014.07.007.

[10] Bilotta A, Ludovico MD, Nigro E. FRP-to-concrete interface debonding: experimental calibration of a capacity model. Composites Part B: Engineering 2011;42(6):1539–53. URL http://dx.doi.org/10.1016/j.compositesb.2011.04.016.

[11] Bilotta A, Faella C, Martinelli E, Nigro E. Design by testing procedure for intermediate debonding in EBR FRP strengthened RC beams. Engineering Structures 2013;46:147–54. URL http://dx.doi.org/10.1016/j.engstruct.2012.06.031.

[12] Monti G, Alessandri S, Santini S. Design by testing: a procedure for the statistical determination of capacity models. Construction and Building Materials 2009;23(4):1487–94. URL http://dx.doi.org/10.1016/j.conbuildmat.2008.07.016.

[13] Monti G, Santini S. Reliability-based calibration of partial safety coefficients for fiber-reinforced plastic. Journal of Composites for Con-

struction 2002;6(3):162–7. URL http://dx.doi.org/10.1061/(ASCE)1090-0268(2002)6:3(162).

[14] Carrara P, Freddi F. Statistical assessment of a design formula for the debonding resistance of FRP reinforcements externally glued on masonry units. Composites Part B: Engineering 2014;66:65–82. URL http://dx.doi.org/10.1016/j.compositesb.2014.04.032.

[15] Gomes S, Neves L, Dias-da Costa D, Fernandes P, Júlio E. Probabilistic models for mechanical properties of prefabricated CFRP. In: 11th fiber reinforced polymers for reinforced concrete structures (FRPRCS11), Guimarães, Portugal. 2013,.

[16] JCSS. Probabilistic model code. The Joint Committee on Structural Safety; 2001.

[17] CNR. Istruzioni per la progettazione, l'esecuzione ed il controllo di interventi di consolidamento statico mediante l'utilizzo di compositi fibrorinforzati. CNR-DT 200 R1/2012; National Research Council, Rome, Italy; 2012.

[18] CSA. Canadian highway bridge design code. CAN/CSA S6-06; Canadian Standards Association, Canada; 2006.

[19] Atadero RA, Karbhari VM. Probabilistic based design for FRP strengthening of reinforced concrete. Special Publication (ACI) 2005;230:723–42.

[20] Zureick A, Bennett R, Ellingwood B. Statistical characterization of fiber-reinforced polymer composite material properties for structural design.

Journal of Structural Engineering 2006;132(8):1320–7. URL http://dx.doi.org/10.1061/(ASCE)0733-9445(2006)132:8(1320).

[21] Zhang S, Yu T, Chen G. Reliability analysis of tensile strengths using Weibull distribution in glass/epoxy and carbon/epoxy composites. Composites Part B: Engineering 2018;133:129–44. URL https://doi.org/10.1016/j.compositesb.2017.09.002.

[22] Seracino R, Jones N, Ali M, Page M, Oehlers D. Bond strength of near-surface mounted FRP strip-to-concrete joints. Journal of Composites for Construction 2007;11(4):401–9. URL http://dx.doi.org/10.1061/(ASCE)1090-0268(2007)11:4(401).

[23] Bilotta A, Ceroni F, Di Ludovico M, Nigro E, Pecce M, Manfredi G. Bond efficiency of EBR and NSM FRP systems for strengthening concrete members. Journal of Composites for Construction 2011;15(5):757–72. URL http://dx.doi.org/10.1061/(asce)cc.1943-5614.0000204.

[24] Kalupahana W. Anchorage and bond behaviour of near surface mounted fibre reinforced polymer bars. Phd thesis; University of Bath, United Kingdom; 2009.

[25] Macedo L, Costa I, Barros J. Assessment of the influence of the adhesive properties and geometry of CFRP laminates in the bond behavior. In: BE2008 - Betão Estrutural 2008. Guimarães, Portugal. 2008,.

[26] Oehlers DJ, Haskett M, Wu C, Seracino R. Embedding NSM FRP plates for improved IC debonding resistance. Journal of Composites for

Construction 2008;12(6):635–42. URL http://dx.doi.org/110.1061/(asce)1090-0268(2008)12:6(635).

[27] Thorenfeldt E. Bond capacity of CFRP strips glued to concrete in sawn slits. In: FRPRCS-8, Patras, Greece. 2007,.

[28] Mitchell P. Freeze-thaw and sustained load durability of near surface mounted FRP strengthened concrete. MSc Thesis, Queens University, Canada; 2010.

[29] Rashid R, Oehlers DJ, Seracino R. IC debonding of FRP NSM and EB retrofitted concrete: plate and cover interaction tests. Journal of Composites for Construction 2008;12(2):160–7. URL http://dx.doi.org/10.1061/(asce)1090-0268(2008)12:2(160).

[30] Seo SY, Feo L, Hui D. Bond strength of near surface-mounted FRP plate for retrofit of concrete structures. Composite Structures 2013;95:719–27. URL http://dx.doi.org/10.1016/j.compstruct.2012.08.038.

[31] Palmieri A, Matthys S, Barros J, Costa I, Bilotta A, Nigro E, et al. Bond of NSM FRP strengthened concrete: round robin test initiative. In: CICE 2012, Rome, Italy. 2012,.

[32] Palmieri A, Matthys S, Taerwe L. Double bond shear tests on NSM FRP strengthened members. In: CICE 2012, Rome, Italy. 2012,.

[33] Teng JG, De Lorenzis L, Wang B, Li R, Wong T, Lam L. Debonding failures of RC beams strengthened with near surface mounted CFRP strips. Journal of Composites for Construction 2006;10(2):92–105. URL http://dx.doi.org/10.1061/(ASCE)1090-0268(2006)10:2(92).

[34] Capozucca R. Analysis of bond-slip effects in RC beams strengthened with NSM CFRP rods. Composite Structures 2013;102:110–23. URL http://dx.doi.org/10.1016/j.compstruct.2013.02.024.

[35] Barros J, Costa I. Bond tests on near surface reinforcement strengthening for concrete structures. Tech. Rep.; Civil Engineering Department, University of Minho, Guimarães, Portugal; 2010.

[36] Shield C, French C, Milde E. The effect of adhesive type on the bond of NSM tape to concrete. In: FRPRCS7, Kansas City, Missouri, USA. 2005, p. 355–72.

List of Figures

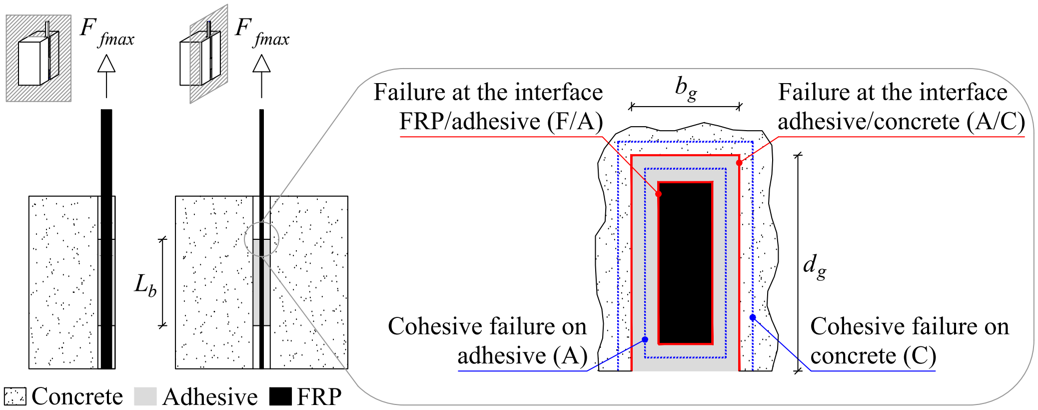

Fig. 1. Example of a direct pullout test specimen and its possible local failure modes.

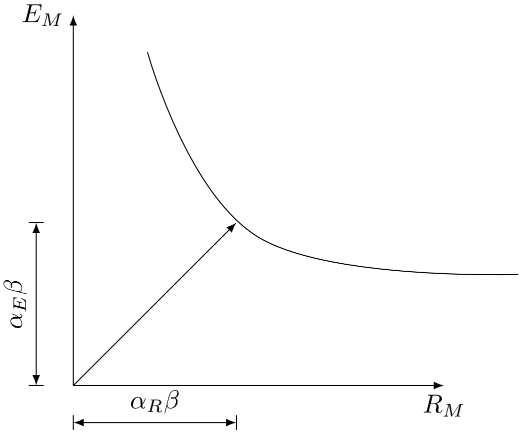

Fig. 2. Design point and reliability index in the normalized space according to FORM.

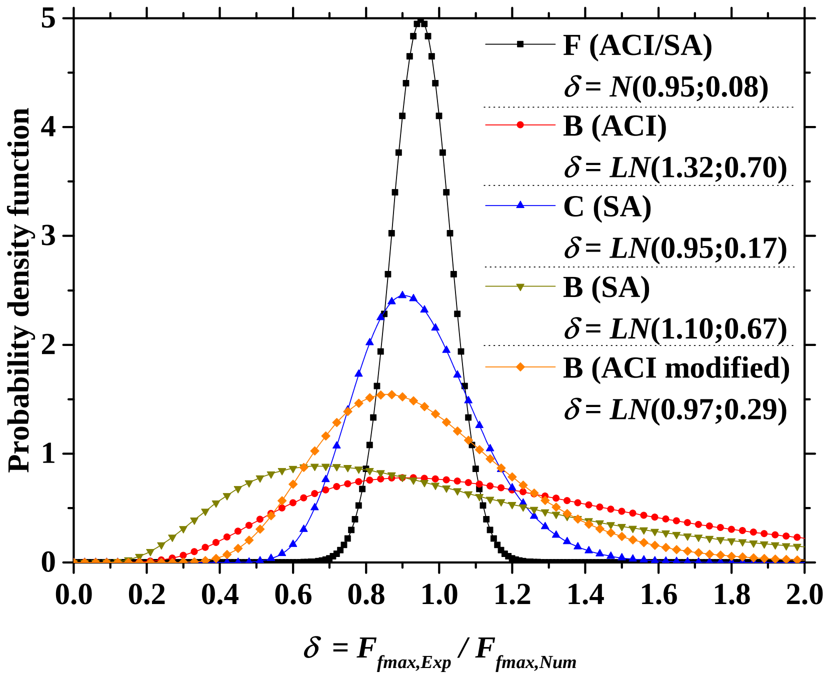

Fig. 3. Probability density function of the error δ associated with each limit state theoretical resistance function.

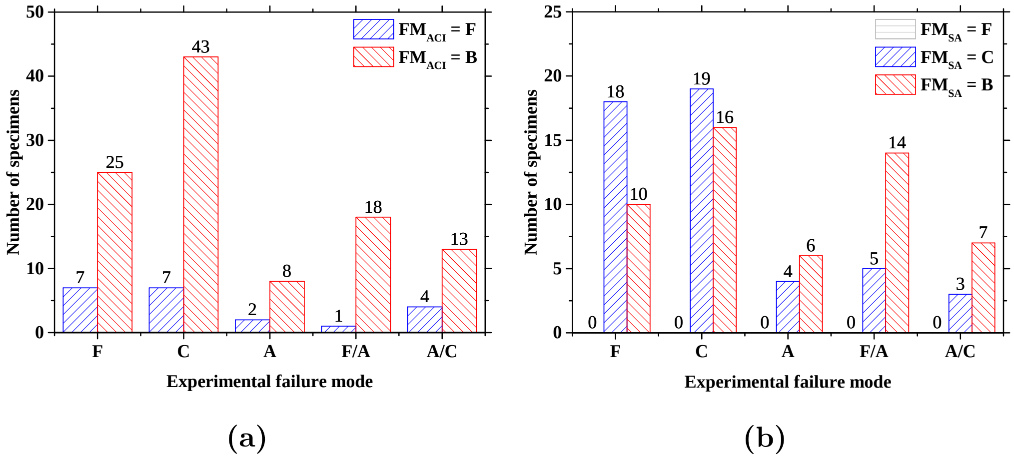

Fig. 4. Failure modes (FM) obtained in the experimental tests *versus* its prediction using the theoretical resistance model defined in: (a) ACI guideline; (b) SA guideline.

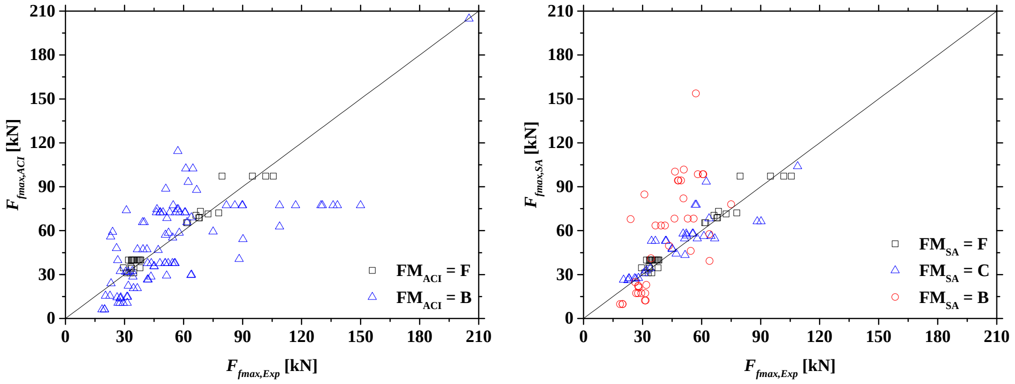

(a) **(b)**

Fig. 5. Experimental *versus* predicted maximum pullout force considering the specimens separately by experimental failure mode (FM) and applying the corresponding limit state function using: (a) ACI guideline; (b) SA guideline.

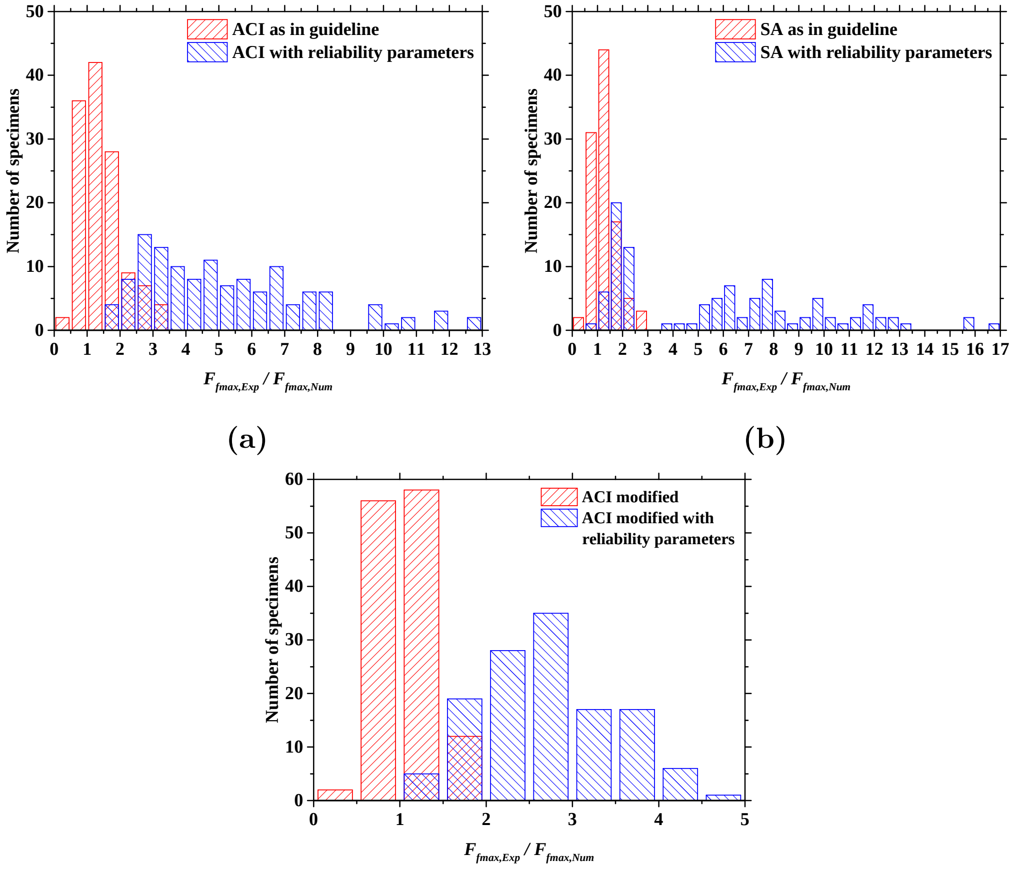

(a)

(b)

(c)

Fig. 6. Histograms of the predictions errors for the resistance models of: (a) ACI guideline; (b) SA guideline; (c) ACI modified.

List of Tables

Table 1. Summary of ACI and SA formulations to estimate NSM FRP systems bond strength.

Parameter	ACI as defined in its guideline	SA as defined in its guideline
Development length [L_d]	$(A_f f_{fd}) / (p_f \tau_{avg})$	$\pi / \left[2\sqrt{(\tau_{max} L_{per}) / (\delta_{max} E_f A_f)}\right]$
Maximum pullout force [F_{fmax}]	$\begin{cases} A_f f_{fd} \text{ if } L_b \geq L_d \\ A_f f_{fd} \frac{L_b}{L_d} \text{ if } L_b < L_d \end{cases}$	$\begin{cases} \sqrt{\tau_{max} \delta_{max} L_{per} E_f A_f} \leq A_f f_{fd} \text{ if } L_b \geq L_d \\ \sqrt{\tau_{max} \delta_{max} L_{per} E_f A_f} \frac{L_b}{L_d} \leq A_f f_{fd} \text{ if } L_b < L_d \end{cases}$
Other relevant information	$\tau_{avg} = 6.9$ MPa	$\tau_{max} = (0.8 + 0.078 \varphi_{per}) f_c^{0.6}$ $\delta_{max} = \left(0.73 \varphi_{per}^{0.5} f_c^{0.67}\right) / \tau_{max}$ $\varphi_{per} = (d_g + 1) / (b_g + 2)$ $L_{per} = 2 (d_g + 1) + b_g + 2$

Table 2. Results obtained in the partial safety factors method.

Limit state	Step in the partial safety factors method described in section 1 [1]				
	(i)		(iii)	(v)	(vi)
	Theoretical resistance function (R_t)	Random variables	Probabilistic resistance function distribution (R)	Design resistance function (R_d)	Safety factors
F (ACI/SA)	Eq. 10	f_{fu}	$\frac{R}{A_f} \sim N(2554.33; 298.18)$[2]	$A_f \frac{f_{fk}}{\gamma_f}$	$\gamma_f = 1.4$
B (ACI)	Eq. 11	-	$\frac{R}{6.9 L_b p_f} \sim LN(1.32; 0.70)$[3]	$\tau_d L_b p_f$	$\tau_d = 1.77$
C (SA)	Eq. 12	$E_f; f_c$	$\frac{R}{\sqrt{0.73 \varphi_{per}^{0.5} L_{per} A_f}} \sim$[2,4]	$\eta_c \sqrt{0.73 \varphi_{per}^{0.5} (\frac{f_{ck}}{\gamma_c})^{0.67} L_{per} E_f A_f}$	[4]
B (SA)	Eq. 13	f_c	$\frac{R}{\frac{2L_b}{\pi}(0.8+0.078\varphi_{per})L_{per}} \sim$[2,4]	$\eta_b \frac{2L_b}{\pi}(0.8 + 0.078\varphi_{per}) L_{per} (\frac{f_{ck}}{\gamma_c})^{0.6}$	[4]
B (ACI modified)	Eq. 14	-	$\frac{R}{162(\frac{A_f}{p_f L_b})^{0.55} L_b p_f} \sim LN(0.97; 0.29)$[3]	$\eta 162 \left(\frac{A_f}{p_f L_b}\right)^{0.55} L_b p_f$	$\eta = 0.38$

[1] step (ii) is depicted in Fig. 3 while step (iv) was achieved by applying Eq. 5 to each distribution of step (iii).

[2] joint probability obtained in 10^6 Monte Carlo simulations using the error δ and the existing random variables.

[3] equal to the error probability distribution (see Fig. 3) since that is the only random variable.

[4] see Table 3.

Table 3. Results obtained in the reliability analyses of SA limit states depending on the concrete class.

Concrete class	Concrete cohesive failure limit state		Debonding limit state	
	Probabilistic resistance function model	η_c	Probabilistic resistance function model	η_b
C12/15	$LN(1088.39; 197.8)$	0.73	$LN(6.62; 4.06)$	0.29
C16/20	$LN(1156.37; 210.15)$	0.71	$LN(7.38; 4.54)$	0.27
C20/25	$LN(1217.96; 220.92)$	0.69	$LN(8.08; 4.96)$	0.26
C25/30	$LN(1287.07; 233.71)$	0.68	$LN(8.92; 5.48)$	0.25
C30/37	$LN(1348.87; 244.79)$	0.67	$LN(9.73; 5.98)$	0.25
C35/45	$LN(1406.82; 255.2)$	0.66	$LN(10.47; 6.44)$	0.24
C40/50	$LN(1458.9; 264.79)$	0.66	$LN(11.2; 6.89)$	0.24
C45/55	$LN(1507.47; 273.62)$	0.65	$LN(11.88; 7.29)$	0.24
C50/60	$LN(1553.57; 281.64)$	0.65	$LN(12.53; 7.71)$	0.23
C55/67	$LN(1597.68; 289.77)$	0.65	$LN(13.18; 8.12)$	0.23

Notation

The following acronyms and symbols are used in this paper:

Acronyms

A	Adhesive cohesive failure mode
ACI	American concrete institute guideline
B	Debonding failure mode (This includes C, A, F/A and A/C in the case of ACI, and A, F/A and A/C in the case of SA)
C	Concrete cohesive failure mode
(C)FRP	(Carbon) Fibre reinforced polymer
EC	Eurocode
F	FRP rupture failure mode
NSM	Near-surface mounted technique
R	Probabilistic resistance function
R_e	Experimental resistance value
R_t	Theoretical limit state resistance function
R_d	Design value of the limit state resistance function
SA	Standards Australia guideline
A/C	Adhesive/concrete interface failure mode
F/A	FRP/adhesive interface failure mode

Symbols

δ	Error
δ_d	Design maximum bond slip
δ_{max}	Maximum bond slip
γ_c	Concrete partial safety factor
γ_f	FRP partial safety factor
η_b	Debonding limit state global safety factor (SA guideline)
η_c	Concrete failure limit state global safety factor (SA guideline)
φ_{per}	Failure perimeter ratio
τ_d	Design bond strength
τ_{avg}	Average bond strength
τ_{max}	Maximum bond strength
A_f	FRP cross-section area
b_g	Groove width
d_g	Groove depth
E_f	FRP modulus of elasticity
f_c, f_{cm}, f_{ck}	Concrete cylinder compressive strength, mean and characteristic values, respectively
F_{fmax}	Maximum pullout force installed in the FRP
$F_{fmax,d}$	Design maximum pullout force installed in the FRP
f_{fu}, f_{fk}, f_d	FRP tensile strength ultimate, characteristic and design values, respectively
L_b	Bonded length
L_d	Development length
L_{per}	SA failure plane perimeter
p_f	FRP perimeter